

Comparison about as-cast microstructures and mechanical properties of Mg–4Y–1.2Mn–0.9Sc and Mg–4Y–1.2Mn–1Zn (wt%) magnesium alloys

Mingbo Yang · Fusheng Pan · Jia Shen ·
Yi Zhu · Caiyuan Qin

Received: 3 October 2010 / Accepted: 10 December 2010 / Published online: 23 December 2010
© Springer Science+Business Media, LLC 2010

Abstract In this article, the as-cast microstructures and mechanical properties of the Mg–4Y–1.2Mn–0.9Sc and Mg–4Y–1.2Mn–1Zn (wt%) magnesium alloys are investigated and compared. The results indicate that the Sc-containing alloy is mainly composed of α -Mg and fine particle-like $Mg_{24}Y_5$, $Mn_{12}Y$, and Mn_2Sc phases, while the Zn-containing alloy mainly consists of α -Mg and coarse $Mg_{12}YZn$ phases with a continuous network. Furthermore, the grains of the Zn-containing alloy are relatively finer than those of the Sc-containing alloy. In addition, the Sc-containing alloy exhibits relatively higher tensile properties at room temperature and 300 °C than the Zn-containing alloy. However, the creep properties at 300 °C and 30 MPa for 100 h for the Sc-containing alloy are relatively lower than those for the Zn-containing alloy.

Introduction

At present, the development of new magnesium alloys is becoming increasingly important due to the potential

saving in weight when compared to aluminum based alloys. However, the creep properties of magnesium alloys are limited by their low melting point which can vary depending on the alloying content [1]. Hence the development of elevated temperature magnesium alloys is necessary in order to compete with other light constructional materials such as aluminum alloys and in order to improve the temperature range of application of magnesium components. Previous investigations indicated that magnesium alloys based on the Mg–Sc system exhibited interesting properties [2, 3], and it was further found that the additions of Mn and Y to Mg–Sc alloys could improve the creep resistance substantially [4, 5]. For example, the quaternary Mg–Y–Mn–Sc alloys are considerably superior to WE alloys (Mg–Y–Nd–Zr) and exhibit high creep resistance at high temperatures over 300 °C [5, 6]. However, due to the expensive scandium, the application of the Mg–Y–Mn–Sc alloys is limited. Therefore, the research of replacing expensive scandium by cheap alloying elements for the Mg–Y–Mn–Sc alloys needs to be considered. Since Zn can form intermetallic phases with Mg and/or RE as plates on basal planes of α -Mg matrix [7], it is inferred that Zn is the possible less expensive alternative to Sc in the Mg–Y–Mn–Sc alloys. But up to now, the investigation whether Sc in the Mg–Y–Mn–Sc alloys can be replaced by Zn, which is very scarce in the literature. Although Smola et al. [7] found that the Mg–4Y–1Mn–1Zn alloy exhibited higher creep properties than the Mg–4Y–1Mn–1Sc alloy, the corresponding information about the comparison of microstructures and mechanical properties for the two alloys, is not reported in detail. Due to the above mentioned-reasons, the present study investigates and compares the as-cast microstructures and mechanical properties of the Mg–4Y–1.2Mn–0.9Sc and Mg–4Y–1.2Mn–1Zn magnesium alloys.

M. Yang (✉) · J. Shen · Y. Zhu · C. Qin
Materials Science & Engineering College, Chongqing University
of Technology, Chongqing 400054, China
e-mail: yangmingbo@cqut.edu.cn

M. Yang · F. Pan
National Engineering Research Center for Magnesium Alloys,
Chongqing University, Chongqing 400030, China

M. Yang
Key Laboratory of Automobile Components Manufacturing
and Testing Technology of the Education Ministry,
Chongqing University of Technology,
Chongqing 400054, China

Experimental procedures

The nominal compositions (wt%) of the experimental alloys investigated in this study are Mg–4Y–1.2Mn–0.9Sc (1[#] alloy) and Mg–4Y–1.2Mn–1Zn (2[#] alloy). The experimental alloys were prepared by adding pure Mg and Zn (>99.9 wt%), and Y, Sc, and Mn were, respectively, added in the form of Mg–17 wt% Y, Mg–2.91 wt% Sc, and Mg–4.38 wt% Mn master alloys made by Hunan Rare Earth Metal & Material Institute in China. The experimental alloys were melted in a crucible resistance furnace and protected by the RJ-2 flux additions (45 wt% MgCl₂ + 37 wt% KCl + 8 wt% NaCl + 4 wt% CaF₂ + 6 wt% BaCl). In order to decrease the melting loss of Y and Sc, the pure Mg, pure Zn, and/or Mg–Mn master alloy were first melted, and then when the melt temperature was around 740 °C, the Mg–Y and/or Mg–Sc master alloys were added into the melt of the experimental alloys. After held at 740 °C for 60 min, the melts of the experimental alloys were homogenized by mechanical stirring at 300 rpm and then poured into a permanent mould which was coated and preheated to 200 °C in order to obtain a casting. The specimens as shown in Fig. 1 were fabricated from the castings for tensile and creep tests. Furthermore, the samples of the experimental alloys were subjected to a solution heat treatment (520 °C/12 h + water cooled) in order to clearly reveal the grain boundaries. Table 1 lists the actual chemical compositions of the experimental alloys, which were inspected by inductively coupled plasma spectroscopy.

In order to analyze the solidification behavior of the experimental alloys, the differential scanning calorimetry (DSC) was carried out by using a NETZSCH STA 449C system equipped with platinum–rhodium crucibles. Samples weighted around 30 mg were heated in a flowing argon atmosphere from 30 to 700 °C for 5 min before being cooled down to 100 °C. The heating and cooling curves were recorded at a controlling speed of 15 °C/min.

The as-cast and solutionized samples of the experimental alloys were etched in 8% nitric acid solution in distilled water and a solution of 1.5 g picric acid, 25 mL

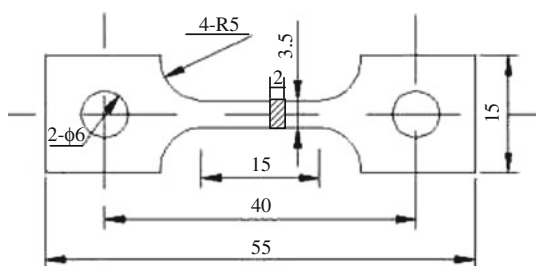


Fig. 1 Configuration of the samples used for the tensile and creep tests (unit:mm)

Table 1 Actual compositions of the experimental alloys, wt%

Experimental alloys	Y	Mn	Sc	Zn	Mg
1 [#] (Mg–4Y–1.2Mn–0.9Sc)	3.66	1.08	0.78	–	Bal.
2 [#] (Mg–4Y–1.2Mn–1Zn)	3.69	1.11	–	0.92	Bal.

ethanol, 5 mL acetic acid, and 10 mL distilled water, respectively, and then examined by an Olympus optical microscope and JOEL JSM-6460LV type scanning electron microscope equipped with Oxford energy dispersive X-ray spectrometer (EDS) with an operating voltage of 20 kV. The grain size was analyzed by the standard linear intercept method using an Olympus stereomicroscope. The phases in the experimental alloys were also analyzed by D/Max-1200X type analyzer operated at 40 kV and 30 mA.

The as-cast tensile properties of the experimental alloys at room temperature and 300 °C were determined from a complete stress–strain curve. Ultimate tensile strength (UTS), 0.2% yield strength (YS), and elongation to failure (Elong.) were obtained based on the average value of three tests. Constant-load tensile creep tests were performed at 300 °C and 30 MPa for creep extension up to 100 h. The minimum creep rates of experimental alloys were measured from each elongation–time curve and averaged over three tests.

Results and discussion

Comparison of microstructures

Figure 2 shows the XRD results of the as-cast alloys. As shown in Fig. 2, the Sc-containing alloy is mainly composed of α -Mg, Mg₂₄Y₅, Mn₁₂Y, and Mn₂Sc phases, similar to the Mg–5Y–1Mn–0.3Sc permanent moulding alloy [8] and the Mg–4Y–1Mn–1Sc squeeze casting alloy [5]. Furthermore, it is found from Fig. 2 that the Zn-containing alloy mainly consists of α -Mg phase and Mg₁₂YZn phase (a long-period 18R modulated structure [9]). Actually, the formation of the phases in the as-cast alloys may be preliminarily explained by the DSC results. Figure 3 shows the DSC cooling curves of the as-cast alloys. It is found from Fig. 3 that the DSC cooling curves of the two alloys are similar, with two main peaks in the cooling curves, corresponding to the α -Mg matrix melting and the eutectic reaction, respectively. Furthermore, it is observed from Fig. 3 that the onset and peak temperatures of the matrix solidification for the two alloys are similar. However, the onset and peak temperatures of second phase transformation for the Sc-containing alloy are higher than those for the Zn-containing alloy. Based on the Mg–Y, Y–Mn, Mg–Y–Mn, and Mg–Mn–Sc phase diagrams [3, 10, 11] and

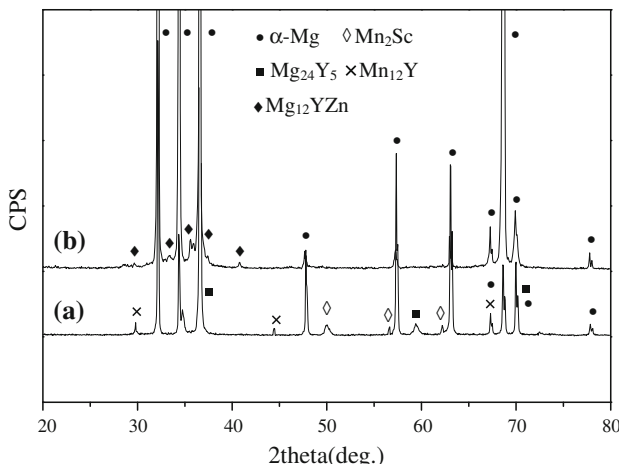


Fig. 2 XRD results of the as-cast alloys: (a) 1# alloy; (b) 2# alloy

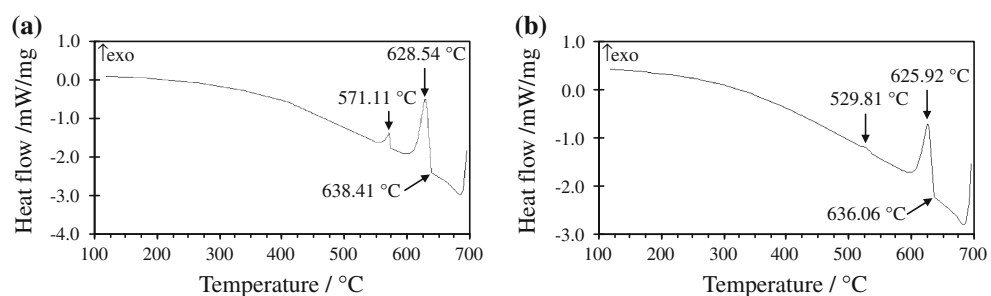
combined with the investigation of Grobner et al. [12], it is preliminarily inferred that during the solidification of the Mg–4Y–1.2Mn–0.9Sc alloy the primary α -Mg phase and Mn₂Sc phase first nucleate and grow until the temperature falls to about 567 °C where a binary eutectic reaction ($L_1 \rightarrow \alpha\text{-Mg} + \text{Mg}_{24}\text{Y}_5$) occurs. Then, along with the temperature decrease the solid solubilities of Y and Mn in the α -Mg solid solution decrease thus results in the solid state precipitation of the Mg₂₄Y₅ and Mn₁₂Y. Accordingly, the final microstructure mainly consists of α -Mg, Mg₂₄Y₅, Mn₁₂Y, and Mn₂Sc phases. As for the Mg–4Y–1.2Mn–1Zn (wt%) alloy with the Y/Zn atomic ratio of 2.94, its solidification process is possibly similar to the Mg–(2–3)Y–1Zn (at.%) alloys reported by Chen and Feng et al. [9, 13]. During the solidification the primary α -Mg phase first nucleates and grows until the temperature falls to about 540 °C where a binary eutectic reaction ($L_1 \rightarrow \alpha\text{-Mg} + \text{Mg}_{12}\text{YZn}$) occurs. Accordingly, the final microstructure is mainly composed of α -Mg and Mg₁₂YZn phases.

Figure 4 shows the SEM images of the as-cast alloys. In Fig. 4, the second phases are identified according to the XRD and EDS analysis. As shown in Fig. 4a, b, the second phases in the Sc-containing alloy mainly exhibit

particle-like shapes, and distribute both at the grain boundary and inside the grains. Furthermore, it is observed from Fig. 4c, d that the Mg₁₂YZn phases in the Zn-containing alloy distribute along the grain boundaries and mainly exhibit continuous network. In addition, although the Mg₂₄Y₅ phase is not identified in the XRD results of the Zn-containing alloy, a small quantity of the Mg₂₄Y₅ phase with particle-like shape is still observed to locate in the Mg₁₂YZn phase (Fig. 4d).

Figure 5 shows the optical images of the as-cast and solutionized alloys. It is observed from Fig. 5a, b that the primary α -Mg phases in the two alloys mainly display a dendrite configuration. Furthermore, it is found from Fig. 5 that the primary α -Mg phases in the Zn-containing alloy are relatively finer than those in the Sc-containing alloy, indicating that the Zn-containing alloy has relatively finer grains than the Sc-containing alloy. This is further confirmed from Fig. 5c, d which shows the solutionized microstructures of the two alloys. The average grain sizes for the Sc and Zn-containing alloys are 324 and 186 μm , respectively. According to the investigations of Fang et al. [14], during solidification the formation of the Mn₂Sc in the Mg–RE–Mn–Sc alloys possibly induces a constitutional undercooling in a diffusion layer ahead of the advancing solid/liquid interface, which restricts the grain growth since the diffusion of the solute slowly occurs. In addition, further nucleation also possibly occurs in front of the interface because nucleants in the melt are more likely to survive and be activated in the constitutional undercooling zone, as reported by Lee et al. [15]. Obviously, the above analysis indicates that the Mg–4Y–1.2Mn–0.9Sc alloy seems to have finer grains than the Mg–4Y–1.2Mn–1Zn alloy. However, as shown in Fig. 5, the contrary results are observed. According to the information from Fig. 4a, c, it is found that the volume fraction of the second phases in the Sc-containing alloy is far less than that in the Zn-containing alloy, indicating that besides forming a small quantity of the second phases, the elements of Y and Sc in the Sc-containing alloy mainly dissolve into the α -Mg matrix. Oppositely, the elements of Y and Zn in the Zn-containing alloy mainly form the second phases

Fig. 3 DSC cooling curves of the as-cast alloys: a 1# alloy; b 2# alloy



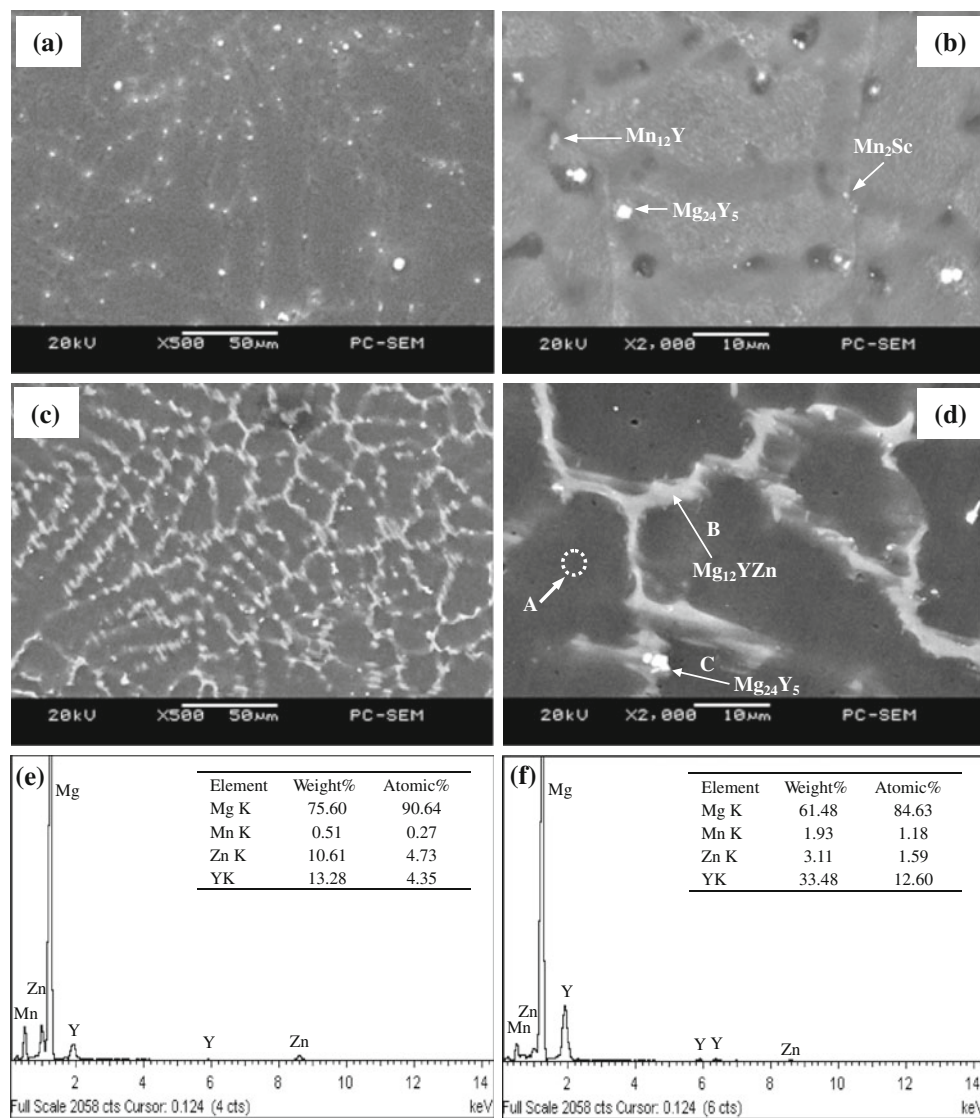


Fig. 4 SEM images of the as-cast alloys: **a, b** 1# alloy; **c, d** 2# alloy; **e** EDS results of position B in **d**; **f** EDS results of position C in **d**

distributed at grain boundaries, which is further confirmed by the EDS analysis. The EDS results of the Zn-containing alloy show that the composition (at.%) of areas A (the matrix), B (the $Mg_{12}YZn$ phase) and C (the $Mg_{24}Y_5$ phase) in Fig. 4d are Mg–0.46Y–0.57Mn–0.25Zn, Mg–4.35Y–0.27Mn–4.73Zn, and Mg–12.6Y–1.18Mn–1.59Zn, respectively. Obviously, Y and Zn elements in the Zn-containing alloy mainly distribute at the grain boundaries, which possibly leads to the Y and Zn enrichments and then induces the constitution undercooling at the solidification interface front during solidification. Based on the above analysis, it is preliminarily inferred that the reason why the Zn-containing alloy has finer grains than the Sc-containing alloy, is possibly related to the formation of the $Mg_{12}YZn$ phase distributed at the grain boundaries for the Zn-containing alloy. However, this needs to be further confirmed.

Comparison of mechanical properties

The tensile properties including ultimate tensile strength (UTS), 0.2% yield strength (YS) and elongation (Elong.), and creep properties of the as-cast alloys are listed in Table 2. It is observed from Table 2 that, although the Sc-containing alloy has relatively higher tensile properties at room temperature and 300 °C than the Zn-containing alloy, the creep properties at 300 °C and 30 MPa for 100 h for the former are relatively lower than those for the latter. It is well known that the presence of fine and uniform phases distributed along the grain boundaries is easier to act as an effective straddle to the dislocation motion thus improving the properties of engineering alloys [16]. Apparently, the coarse continuous $Mg_{12}YZn$ phases in the Zn-containing alloy will give a detrimental effect on the tensile properties.

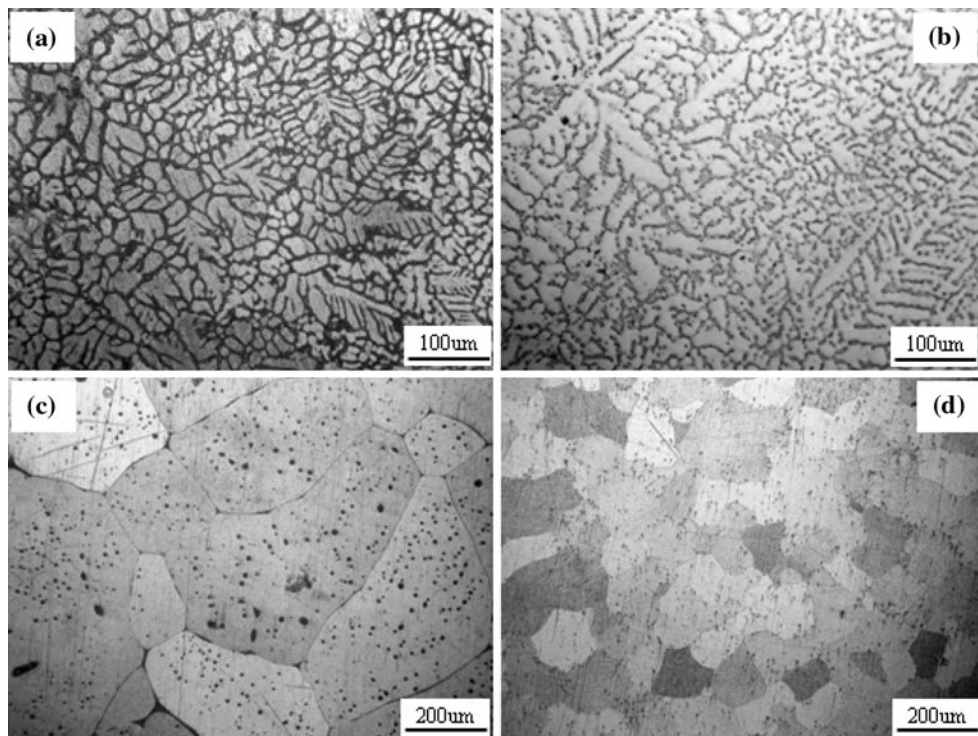


Fig. 5 Optical images of the as-cast and solutionized alloys: **a, c** 1[#] alloy; **b, d** 2[#] alloy

Table 2 Tensile and creep properties of the as-cast alloys

Experimental alloys	Tensile properties						Creep properties	
	Room temperature			300 °C			300 °C and 30 MPa for 100 h	
	UTS/MPa	YS/MPa	Elong./%	UTS/MPa	YS/MPa	Elong./%	Total creep strain/%	Minimum creep rate/ $\times 10^{-9}$ s ⁻¹
1 [#] alloy	194 (4.2)	176 (3.6)	3.6 (0.27)	129 (3.1)	112 (2.9)	17.0 (0.96)	0.343 (0.11)	9.52 (0.21)
2 [#] alloy	182 (3.7)	166 (2.9)	2.8 (0.31)	115 (3.2)	108 (3.3)	14.2 (0.78)	0.312 (0.08)	8.67 (0.18)

Note The data in the bracket is the standard error

Although the Zn-containing alloy has relatively finer grains than the Sc-containing alloy, the presence of these coarse Mg₁₂YZn phases with a continuous network possibly promote the initiation and propagation of cracks and leads to an adverse effect on the tensile properties. This can be further confirmed from Figs. 6 and 7. Figures 6 and 7 show the SEM images of tensile fractographs and optical images of longitudinal sections for the as-cast alloys failed in the tensile tests at room temperature, respectively. As shown in Fig. 6, a number of cleavage planes and steps are present, and some river patterns can also be observed in the tensile fracture surfaces of the experimental alloys, indicating that the tensile fracture surfaces of the two alloys have mixed characteristics of cleavage and quasi-cleavage fractures. However, it is observed from Fig. 7 that, different from the Sc-containing alloy, the tensile rupture of the Zn-containing

alloy occurs along the grain boundaries, and as reported by Luo et al. [17], the cracks seem to preferentially initiate and propagate at interior of the coarse Mg₁₂YZn phase instead of the interface between the Mg₁₂YZn particle and α -Mg matrix due to that the Mg₁₂YZn phase has the axis-to-axis orientation with magnesium matrix, and thus results in the relatively poor tensile properties of the Zn-containing alloy.

In general, it is accepted that the rate of dislocation creep tends to decrease with increasing grain size due to a lowered contribution of grain boundary sliding [18]. Since the grain size of the Zn-containing alloy is smaller than that of the Sc-containing alloy, the difference in the grain size can not explain the higher creep properties of the Zn-containing alloy than the Sc-containing alloy. The difference in the creep properties for the two alloys is possibly related to other reasons. Figure 8 shows the SEM images of

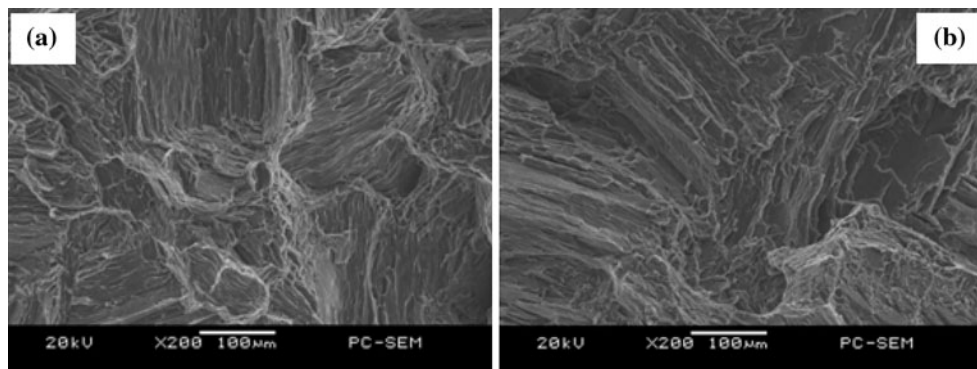


Fig. 6 SEM images of the tensile fractographs for the as-cast alloys tested at room temperature: **a** 1[#] alloy; **b** 2[#] alloy

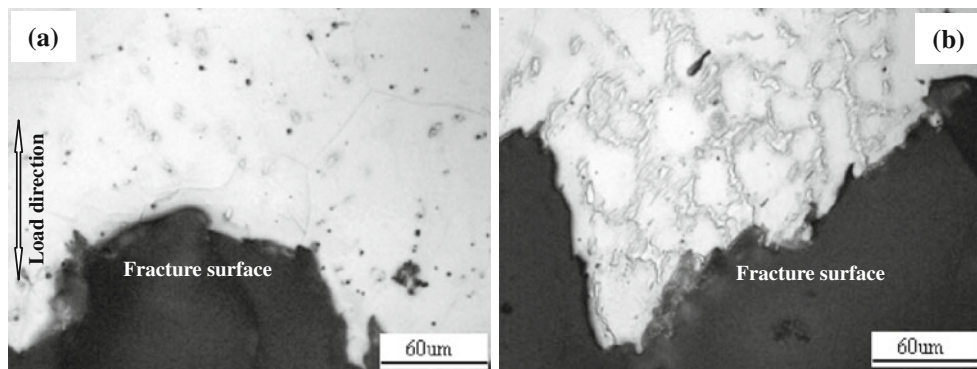


Fig. 7 Optical images of longitudinal sections for the as-cast alloys failed in tensile test at room temperature: **a** 1[#] alloy; **b** 2[#] alloy

the Sc and Zn-containing solutionized alloys. It is observed that, after solid solution heat treatment at 520 °C for 12 h, many remanent second phases are clearly observed in the Sc and Zn-containing alloys, indicating that the structure stability at high temperatures for the two alloys is very high thus leads to the high creep properties of the two alloys (Table 2). However, it is further found from Fig. 8 that the volume fraction of the remanent second phases in the Zn-containing solutionized alloy is more than that in the Sc-containing solutionized alloy, and in the Zn-containing solutionized alloy some coarse remanent second phases with a continuous and/or quasi-continuous networks still distribute along the grain boundaries. Since the creep resistance properties of magnesium alloys are mainly related to the structure stability at high temperatures, the Zn-containing alloy exhibits relatively higher creep properties than the Sc-containing alloy. Based on the above analysis, it is preliminarily inferred that the higher creep properties of the Zn-containing alloy than the Sc-containing alloy are possibly related to the different initial as-cast microstructures of the two alloys. However, this needs to be further confirmed.

In addition, it is well known that the high creep properties for Mg–RE–Mn–Sc alloys are mainly caused by the

dense dispersion of fine Mn₂Sc particles and then an aging treatment is commonly necessary to the Mg–RE–Mn–Sc alloys in order to produce a fine dispersion of Mn₂Sc phase [19]. Therefore, although the above results indicate that the as-cast creep properties of the Sc-containing alloy are lower than those of the Zn-containing alloy, one question whether the creep properties after an aging treatment for the Sc-containing alloy are also lower than those for the Zn-containing alloy, still remains. This question is a subject for further study in our group.

Conclusions

The as-cast Mg–4Y–1.2Mn–0.9Sc alloy is mainly composed of α -Mg and fine particle-like Mg₂₄Y₅, Mn₁₂Y and Mn₂Sc phases, while the as-cast Mg–4Y–1.2Mn–1Zn alloy mainly consists of α -Mg and coarse Mg₁₂YZn phase with a continuous network. Furthermore, the grains of the Zn-containing alloy are relatively finer than those of the Sc-containing alloy. In addition, the Sc-containing alloy exhibits relatively higher tensile properties at room temperature and 300 °C than the Zn-containing alloy. However, the creep properties at 300 °C and 30 MPa for 100 h

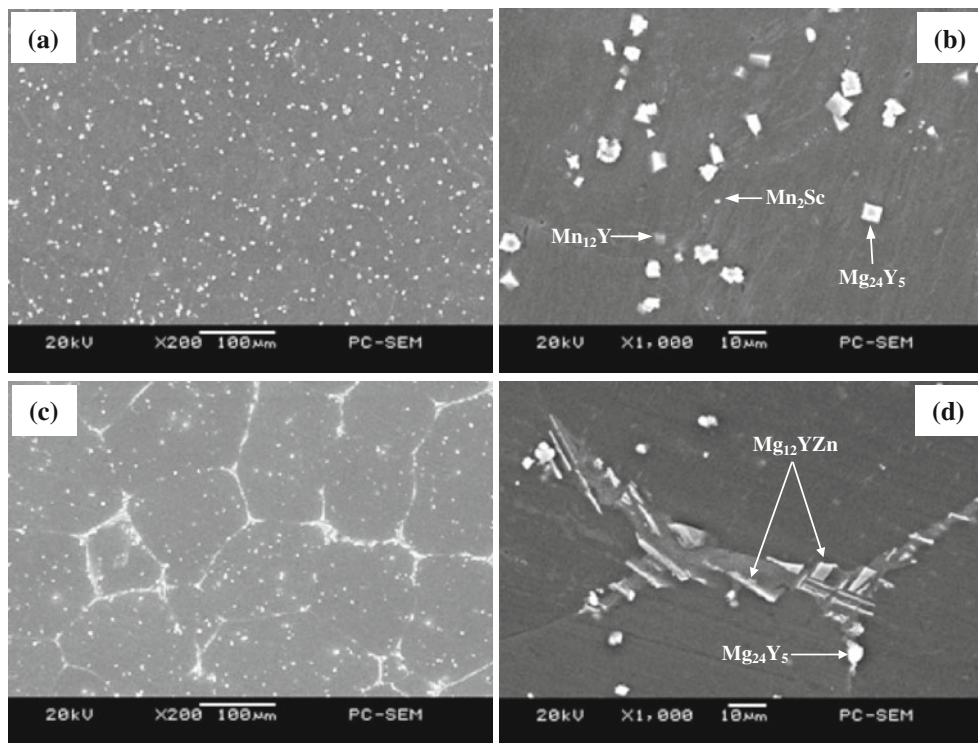


Fig. 8 SEM images of the solutionized alloys: **a, b** 1[#] alloy; **c, d** 2[#] alloy

for the Sc-containing alloy are relatively lower than those for the Zn-containing alloy.

Acknowledgements The present study was supported by the National Natural Science Funds of China (No. 50725413), the Major State Basic Research Development Program of China (973) (No. 2007CB613704), the Chongqing Science and Technology Commission in China (CSTC, 2010AC4085, 2009AB4134 and 2006AA4012-9-6), the Chongqing Education Commission in China (KJ090628) and the Program for Hundreds of Distinguished Leading Scientists of CQ CSTC (2010CSTC-HDLS).

References

1. Luo A, Pekguleryuz MZ (1994) J Mater Sci 29:5259. doi: [10.1007/BF01171534](https://doi.org/10.1007/BF01171534)
2. Mordike BL, Stulikova I, Smola B (2005) Metal Mater Trans A 36:1729
3. Buch FV, Lietzau J, Mordike BL, Pisch A, Schmid-Fetzer R (1999) Mater Sci Eng A 263:1
4. Mordike BL (2001) J Mater Proc Technol 117:391
5. Stulikova I, Smola B, Buch FV, Mordike BL (2003) Materialwissenschaft und Werkstofftechnik 34:102
6. Smola B, Stulikova I, Pelcova J, Mordike BI (2004) J Alloys Compd 378:196
7. Smola B, Stulikova I, Pelcova J, Zaludova N (2007) Phase composition and creep behavior of Mg–RE–Mn alloys with Zn addition [A]. In: Kainer KU (ed) Proceedings of 7th international conference on magnesium alloys and their applications[C], Dresden, Germany, 2007, pp 67–72
8. Xiong CX, Zhang XM, Jiang H (2006) Heat Treat Met (in Chinese) 31:53
9. Chen B, Lin DL, Zeng XQ, Lu C (2010) J Mater Sci 45:2510. doi: [10.1007/s10853-010-4223-z](https://doi.org/10.1007/s10853-010-4223-z)
10. Kang Y-B, Pelton AD, Chartrand P, Spencer P, Fuerst CD (2007) Metal Mater Trans A38:1231
11. Pisch A, Antion C, Tassin C, Baillet F, Grobner J, Schmid-Fetzer R (2006) Phase equilibria, microstructure and properties of novel Mg–Mn–Y alloys [A]. In: Kainer KU (ed) Proceedings of 6th international conference on magnesium alloys and their applications [C], Geesthacht, Germany, 2006, pp 78–82
12. Grobner J, Schmid-Fetzer R (2001) J Alloys Compd 320:296
13. Feng GN, Guo XF, Xu CJ, Zhang ZM (2006) J China Rare Earth Soc 24:86
14. Fang XY, Yi DQ, Nie JF, Zhang XJ, Wang B, Xiao LR (2009) J Alloys Compd 470:311
15. Lee YC, Dahle AK, Stjohn DH (2000) Metal Mater Trans A 31:2895
16. Balasubramani N, Pillai UTS, Pai BC (2008) J Alloys Compd 457:118
17. Luo ZP, Zhang SQ (2000) J Mater Sci Lett 191:813
18. Zhu SM, Mordike BL, Nie JF (2008) Mater Sci Eng A 483–484:583
19. Fang XY, Yia DQ, Nie JF (2009) J Alloys Compd 486:900